Geophysical Research Letters®

Key Points:

- Auroral acceleration is modeled by considering magnetic reconnection in the field-aligned current sheet
- Periodic spiral structures can develop from an auroral arc modified by secondary oblique tearing instability
- The characteristics of the spiral structures in our simulation agree well with observation

Supporting Information:

Supporting Information may be found in the online version of this article.

Correspondence to:

Y.-H. Liu and Q. Lu,
Yi-Hsin.Liu@dartmouth.edu;
qmlu@ustc.edu.cn

Auroral Spiral Structure Formation Through Magnetic Reconnection in the Auroral Acceleration Region

Kai Huang[1,2] ![ORCID], Yi-Hsin Liu[3] ![ORCID], Quanming Lu[1,2] ![ORCID], Zejun Hu[4] ![ORCID], Kristina A. Lynch[3] ![ORCID], Michael Hesse[5] ![ORCID], Andris Vaivads[6] ![ORCID], and Huigen Yang[4] ![ORCID]

[1]CAS Key Lab of Geospace Environment, School of Earth and Space Sciences, University of Science and Technology of China, Hefei, China, [2]CAS Center for Excellence in Comparative Planetology, Hefei, China, [3]Department of Physics and Astronomy, Dartmouth College, Hanover, NH, USA, [4]MNR Key Laboratory for Polar Science, Polar Research Institute of China, Shanghai, China, [5]NASA Ames Research Center, Moffett Field, CA, USA, [6]Department of Space and Plasma Physics, School of Electrical Engineering and Computer Science, KTH Royal Institute of Technology, Stockholm, Sweden

Abstract Auroral spiral is one of the auroral vortex structures. Here, we propose a model to explain the formation of auroral spiral structure based on three-dimensional particle-in-cell simulations. In our model, an auroral arc develops through precipitations of electrons accelerated during magnetic reconnection in the auroral acceleration region. The arc morphology at low altitudes can be modified by electron-scale magnetic flux ropes, which are generated through secondary oblique tearing modes in the intensified current sheet along one particular branch of the primary reconnection separatrices. The resulting vortex structures agree well with high-resolution observations of auroral spirals. We find that the rotational sense of these spirals is determined by electron kinetic processes and controlled by the guide field direction. Our study further suggests that when the field-aligned length of the auroral acceleration region is shorter than a critical length, these auroral spiral structures will not form.

Plain Language Summary Discrete aurorae, usually displayed as auroral arcs, are universal phenomena in the ionosphere of the Earth and other planets, and are generated by precipitations of electrons from the magnetosphere, ionosphere, and solar wind. Spirals, as frequently observed vortex structures in arcs, have drawn great attention. The formation of auroral spirals is considered to be related to the magnetosphere-ionosphere coupling process during both magnetically active and quiet times. However, how the auroral spirals develop is still an open question. It is suggested that magnetic reconnection occurs in the auroral acceleration region, typically above ~4,000 km altitude in the field-aligned current sheet. Using kinetic simulations, we study the role of magnetic reconnection in the formation of auroral spirals.

1. Introduction

Discrete auroral arcs in the ionosphere usually display as geomagnetically east-west aligned narrow structures, and are associated with an upward field-aligned current (FAC) carried mainly by the downward-accelerated electrons originating from the magnetosphere (Borovsky et al., 2020; Paschmann et al., 2002). A stable arc can often be distorted and evolve into more complex shapes, such as spirals, folds, and curls (Hallinan, 1976). Auroral spiral is one of the representative auroral vortex structures, which appears either as an isolated vortex or as a vortex array. The diameter of a spiral ranges from 15 to 1,300 km, and the typical value is around 25–75 km. Importantly, the spirals rotate clockwise (anti-clockwise) in the sky-view at the northern (southern) hemisphere. The rotational sense is always clockwise when viewed in the direction anti-parallel to the geomagnetic field, but the reason remains poorly understood (Davis & Hallinan, 1976; Partamies, Kauristie, et al., 2001).

Two types of theories had been developed to explain how the auroral spirals form. One links the spirals to instabilities in the FAC sheet (Hallinan, 1976; Lysak & Song, 1996; Otto & Birk, 1992; Partamies, Freeman, & Kauristie, 2001). Hallinan (1976) attributed the formation of auroral spirals to current sheet instability where the geomagnetic field lines twist due to the high altitude perturbation in the FAC sheet. Lysak and Song (1996) explored the coupling of Kelvin-Helmholtz instability at a high altitude and the current sheet instability as a function of height-integrated ionospheric conductivity, showing that the ionospheric feedback can alter the rotational pattern in their model. Otto and Birk (1992) proposed that auroral spirals may relate to the small-scale filamentation of auroral arcs caused by resistive tearing instability in the FAC sheet. The other type of theory considers magne-

Table 1
Estimated Parameters in the Auroral Acceleration Region

Quantity name	Estimated value
Geomagnetic field	10^4 nT
Reconnecting magnetic field	100 nT
Plasma number density	1 cm^{-3}
Electron temperature	2 keV
Ion inertial length	230 km
Electron inertial length	5 km
Inversed ion gyrofrequency	0.1 s

tospheric dynamics as the driver of spirals, such as the Kelvin-Helmholtz instability at the magnetopause (Hu et al., 2013; Johnson et al., 2014; Lui et al., 1989) and magnetotail dynamics (Elphinstone et al., 1995; Keiling, Angelopoulos, Runov, et al., 2009; Keiling, Angelopoulos, Weygand, et al., 2009; Murphree & Elphinstone, 1988). However, to date, there is no consensus on the formation mechanism of auroral spirals, and a satisfactory explanation of their rotational sense remains elusive.

It is suggested that magnetic reconnection can occur in the auroral acceleration region, which is typically above ∼4,000 km altitude in the FAC sheet (Chaston, 2015; Lanchester, 2017; Seyler, 1990). These upward FAC sheets are driven by large scale processes from the magnetosphere, such as a convection flow above the auroral zone and flow channels from the magnetotail (Borovsky et al., 2020). In this paper, by performing three-dimensional (3-D) particle-in-cell (PIC) simulations of magnetic reconnection designed to model the auroral acceleration region, we provide a promising explanation for auroral spiral structure formation along an arc.

2. Simulation Setup

Our simulations are performed using the 3-D PIC code VPIC (Bowers et al., 2008). To study magnetic reconnection in the auroral acceleration region, x, y, and z represents the longitude, (field-aligned) altitude, and latitude of Earth's geographic coordinate. The initial condition is a force-free current sheet with magnetic field $\mathbf{B} = B_0 \tanh(z/\delta_0)\mathbf{e}_x - B_0\sqrt{\mathrm{sech}^2(z/\delta_0) + B_g^2/B_0^2}\mathbf{e}_y$, where δ_0 is the half-thickness of the initial current sheet and B_g is the amplitude of the guide field. The initial density n_0 is uniform. Here, we use $\delta_0 = 0.5d_i$ and $B_g = B_0$ where $d_i = c(\varepsilon_0 m_i/n_0 e^2)^{1/2}$ is the ion inertial length. The plasma beta is $\beta = 2\mu_0 n_0 k(T_{i0} + T_{e0})/(B_0^2 + B_g^2) = 0.1$, where the initial ion and electron temperature $T_{i0} = T_{e0} = T_0$. We use the Alfvén speed $V_A \equiv B_0/(\mu_0 m_i n_0)^{1/2}$ and ion gyro-frequency $\Omega_i \equiv eB_0/m_i$ for the normalization. The ion to electron mass ratio $m_i/m_e = 25$, and the speed of light $c = 10V_A$. An initial perturbation $\delta B_z = 0.05B_0$ is used to induce reconnection. Simulations are performed within boxes of size $L_x \times L_y \times L_z = 32d_i \times 32d_i \times 16d_i$ and $640 \times 640 \times 320$ cells. Over 1.3×10^{10} particles for each species are used. The boundary conditions are periodic in the x-direction, while in the z-direction they are conducting for fields and reflecting for particles. To mimic the conditions in the auroral acceleration region, in the y-direction, we use open boundary condition for particles. On the $-y$ boundary, line-tied boundary are employed for electromagnetic field, while in the $+y$ boundary, open boundary are used (Daughton et al., 2006; Sauppe & Daughton, 2018).

Table 1 lists some estimated parameters in the auroral acceleration region (Ergun, Carlson, McFadden, Delory, et al., 2000; Ergun, Carlson, McFadden, Mozer, & Strangeway, 2000). Based on these parameters, the length of our simulation domain is around 7,000 km in the y-direction, with the $-y$ boundary corresponding to the bottom of the auroral acceleration region (∼4,000 km altitude). We use a small B_g/B_0 value because the expensive computation for realistic 3-D PIC simulations cannot yet be accommodated in modern supercomputers, but the key conclusion derived from reconnection properties is expected to carry over to the large B_g/B_0 limit.

3. Results

Figure 1 shows the evolution of the FAC density $J_∥$ and electron energy flux Γ on the $y = 1d_i$ plane. Here, $B_y < 0$, therefore the $x - z$ plane represents the sky-view at northern latitudes. $J_∥$ is mainly carried by electrons moving to the $-y$ direction along $\mathbf{B}$. The electron energy flux $\Gamma = -\int v_y \varepsilon \mathrm{d}n$ is calculated using electrons with velocity $v_y < 0$ and energy $\varepsilon > 10T_0$. The electron energy flux mimics the morphology of the visible aurora arc. Initially (Figure 1a), the thickness of the current sheet is on the ion inertial scale. The flux of energetic electrons Γ is very low, and no visible arc can be observed. As reconnection proceeds, a thin electron scale current sheet forms near the reconnection x-line and extends to the lower-left and upper-right quadrants of the $x - z$ plane. In the electron scale current sheet, the energy flux of precipitating electrons is enhanced by an order of magnitude, resembling the formation of an auroral arc. Then, both the thin current sheet and the auroral arc extend along the x direction. The arc gradually rolls up (Movie S1), and nine spirals (in the red circles) are generated along the arc at $\Omega_i t = 30$.
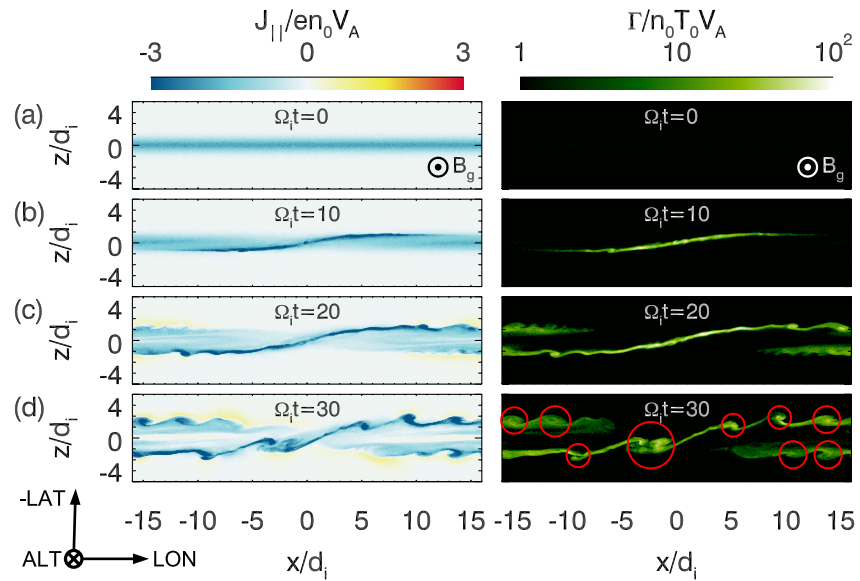
Figure 1. The field-aligned current density $J_\parallel$ and electron energy flux Γ on the $y = 1d_i$ plane at $\Omega_i t = 0$, 10, 20, and 30 respectively.

All of the spirals winding clockwise when viewed along the direction anti-parallel to the guide field B_g, consistent with the definition of auroral spirals in Davis and Hallinan (1976).

The diameter of our simulated spirals is about several times the thickness of the arc, or tens of d_e ($d_e \approx 5$ km is the electron inertia length if we assume the density is 1 cm^{-3}). Considering the geomagnetic mapping from the bottom of auroral acceleration region (~4,000 km) to the ionosphere, the spatial scale of these structures will be compressed (Weimer & Gurnett, 1993) by a factor of $2 \sim 3$. Therefore, our simulation predicts the size of the spiral to be tens of kilometers, consistent with the observations in Partamies, Kauristie, et al. (2001). Hereafter, we will further discuss the origin of these simulated spiral structures.

Panel (a) in Figure 2 shows the magnetic field B_z/B_0 on $y/d_i = 31$, 16, and 1 planes at time $\Omega_i t = 30$. At the lower altitude, a chain of small scale bipolar B_z structures forms. These structures are flux ropes and coincide with the spirals in Figure 1. To show this, panel (d) plots the 3-D magnetic field lines of five selected flux ropes and the contour of J_y on the $y = 0$ plane. In light of these simulation results we propose that the auroral spirals develop in a similar manner due to the electron precipitation along the flux ropes. To confirm the origin of these flux ropes, in panel (b), we use fast Fourier transform (FFT) to study the spectrum of the perturbed magnetic field B_z in the wave number space. The spectrum is calculated on the $x - y$ plane and averaged between $-2d_i < z < 2d_i$. The two circles in panel (b) denote the modes with the maximum growth rate of tearing instability $k\delta \approx 0.5$, where the half-thickness of the current sheet $\delta = 1 \sim 2d_e$. We find that between the two circles, the spectrum of B_z has large values in the region with oblique angle $|\theta| = |\tan^{-1}(k_y/k_x)| < \theta_c = \tan^{-1}(B_0/B_g) = 45°$ (labeled by the diagonal dashed lines) for $B_g = B_0$, indicating the development of the oblique tearing instability (Daughton et al., 2011; Y. H. Liu et al., 2013). Note that for a larger B_g/B_0 ratio, θ_c is smaller. The intense power spectral density in the inner circle is from the large scale B_z produced by the primary x-line. Using the tearing theory in Y. H. Liu et al. (2013), we obtain the theoretical growth rate of oblique tearing mode with $k\delta = 0.5$ in different oblique angles (red curve in panel (c)). The blue curve represents the average power spectral density of B_z as a function of θ from panel (b) between the two circles. The modes are unstable only within the predicted cutoff angle $\theta_c = 45°$, as expected for oblique tearing modes in this simulation. From the maximum growth mode $k\delta \sim 0.5$, we obtain that the wavelength satisfies $\lambda/2\delta \sim 6$. It can be considered reasonable for explaining the spiral observations ($\lambda/2\delta \sim 20$ in Davis and Hallinan (1976)) since $\lambda/2\delta$ will increase (by a factor of $2 \sim 3$) when mapped to the ionosphere (Hallinan, 1976).

In Figure 2d, it is evident that most of the flux ropes only develop at the lower altitude (Huang, Liu, et al., 2020; Y. H. Liu et al., 2019). We run another case with smaller y-domain $L_y = 8d_i$ (Figure S1 in Supporting Information S1), and found no flux rope developing. This comparison suggests that the length of the auroral acceleration region
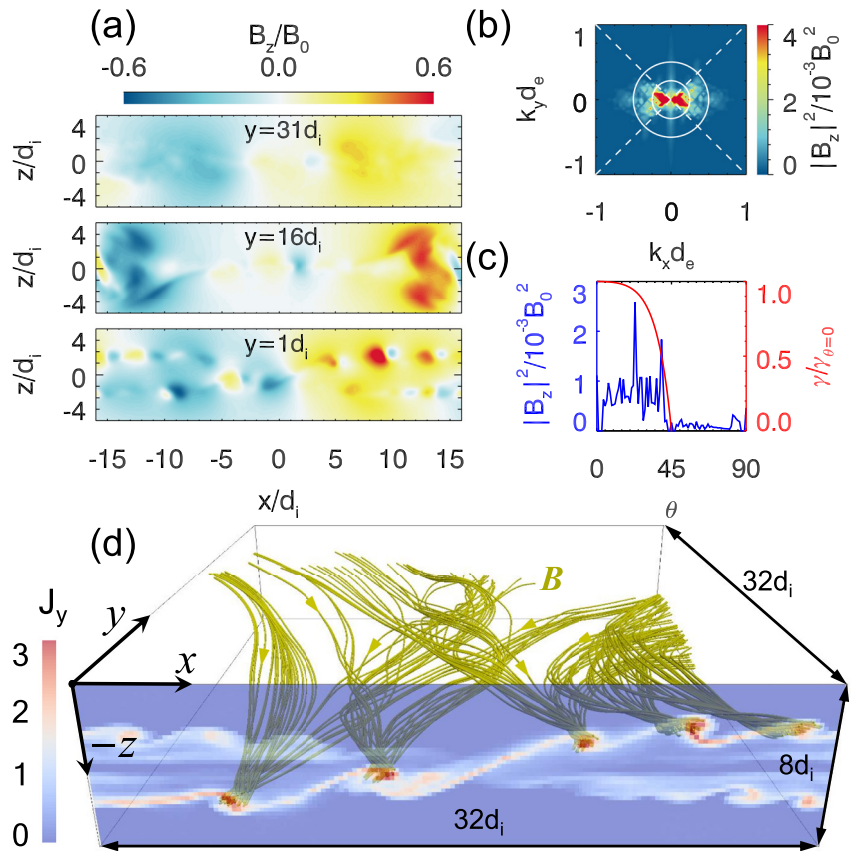
Figure 2. At time $\Omega_i t = 30$. Panel (a) shows the magnetic field B_z on $y/d_i = 31$, 16, and 1 planes. Panel (b) shows the power spectral density of B_z in $k_x - k_y$ space. Panel (c) shows the average power spectrum density of B_z within $0.25 < kd_e < 0.5$ versus the oblique angle θ (blue curve), and the theoretical growth rate of oblique tearing modes with $k\delta = 0.5$ (red curve). Panel (d) shows the 3-D magnetic field lines of five selected flux ropes and the contours of current density J_y on the $y = 0d_i$ plane.

(i.e., the primary reconnection x-line in our model) plays a critical role in determining whether auroral spiral structures can develop. If the auroral acceleration region is too short, no flux rope or spiral will form. The formation of flux ropes requires the current sheet being sufficiently long in the electron streaming direction so that tearing instability can grow through electron resonance (Drake & Lee, 1977) before electrons escape from the acceleration region. The critical length is estimated to be $l_c \sim V_s/\gamma$, where $V_s = J/en = B_0/\mu_0 en\delta$ is the electron streaming speed along the anti-current direction and γ is the growth rate of tearing instabilities. We estimate γ using the predicted maximal growth rate (Y. H. Liu et al., 2013) with $k\delta = 0.5$ and $\theta \simeq 0$, which gives $\gamma\delta \sim (d_e/\delta)^2 v_{eth} B_0/B_g$. Here, B_g represents the geomagnetic field, and v_{eth} is the electron thermal velocity. We then obtain the critical length

$$l_c \sim \left(\frac{\delta}{d_e}\right)^2 \frac{B_g}{\mu_0 en v_{eth}}. \tag{1}$$

Using typical values in Table 1 and $\delta = 2d_e$, then $l_c \sim 10^4$ km. It is comparable to previous estimations of the field-aligned length of the auroral acceleration region (Karlsson et al., 2020). If l_c is too short or too long, the occurrence rate of spirals would be much higher or lower, explaining the moderate occurrence rate of spirals (30% of the DMSP images in Davis and Hallinan (1976)). It was also suggested by Hallinan (1976) and Partamies, Freeman, and Kauristie (2001) that the formation of spiral is affected by the field-aligned length of the FAC. In their model, a longer FAC and a stronger FAC perturbation are in favor of the increased winding of spirals.

The key idea of the auroral spiral structure formation mechanism through secondary oblique tearing instabilities during reconnection is sketched in Figure 3. Panel (a) shows the formation of an auroral arc (solid black curve)
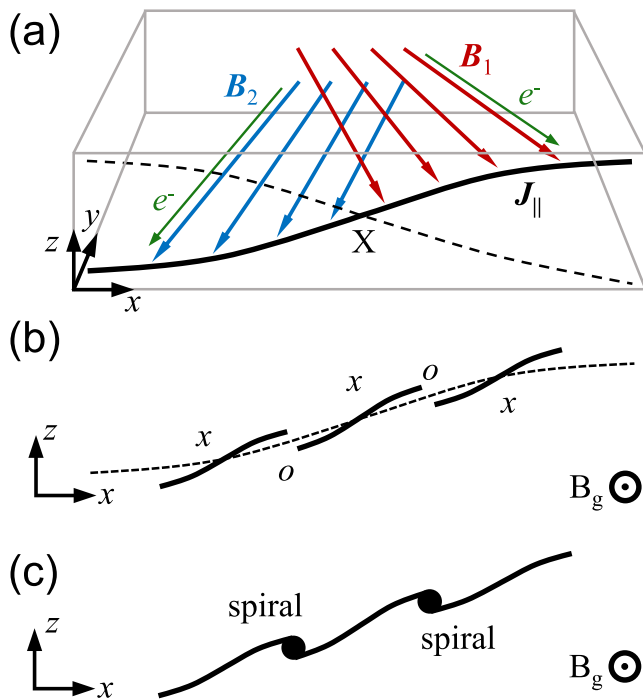
Figure 3. The schematic of the formation mechanism of auroral spirals. Panel (a) illustrates the primary x-line ("X"), where the current density ($J_\parallel$) is intensified along the lower-left/upper-right separatrices (thicker black curve). Panel (b) denotes the secondary x-lines ("x") and o-lines ("o") associated with oblique tearing modes. Panel (c) illustrates the resulting spirals.

during the primary magnetic reconnection. When there is a strong guide field, electrons within the primary x-line at the higher altitude are accelerated by $E_\parallel$ and guided by the shear magnetic fields (B_1 and B_2 on two sides of the FAC sheet) toward the lower-left and upper-right separatrices at the lower altitude. Therefore, the current density ($J_\parallel$) along these separatrices is intensified. This is the electron kinetic signature of magnetic reconnection commonly observed in kinetic simulations (Eastwood et al., 2018; Huang, Lu, et al., 2020; Kleva et al., 1995; Le et al., 2013; Lu et al., 2011; Pritchett & Coroniti, 2004), as also seen in Figure 1. This intensified current sheet is unstable to secondary oblique tearing modes in 3-D, forming a chain of secondary x-lines and flux ropes (o-lines). Similar to panel (a), the current density on the lower-left and upper-right separatrices of these secondary x-lines are also intensified, depicted as the short solid curves in panel (b). As a result, the intensified current sheet in panel (a) is distorted to the shape shown in panel (c), and electrons energized during reconnection will be funneled into these flux ropes, forming auroral spirals. When the direction of the guide field reverses, the intensified current sheet will appear along the upper-left to lower-right separatrices instead (Figure S2 in Supporting Information S1), and the rotational sense of spirals will also reverse.

In Figure 4, we compare simulation results with a coordinated conjunction between the auroral spiral imaging by the Yellow River Station (Hu et al., 2009) and in-situ observations by the DMSP satellite (Hardy, 1984; Rich, 1994) above this spiral. In panel (a), the satellite crosses the spiral (A to B), and then the spiral arm (C to E). The optical image of this spiral is shown at time B (13:49:41 UT), images at A, C-E are shown in Figure S3 in Supporting Information S1. A comparison between the evolution of the observed and simulated spiral can be found in Movie S2. Points A to E in panel (f) denote the positions within our simulation that are comparable to those in the observations. The spiral is characterized by the precipitation of energetic electrons and velocity shears at positions B and D, corresponding to the spiral and spiral arm. The shear flow pattern induces electric fields ($\mathbf{E} = -\mathbf{V} \times \mathbf{B}$) pointing toward the arc, in agreement with previous observations (Marklund et al., 1998). At A and C, where the energy flux of precipitating electrons is low on the two flanks of the spiral, the ion velocities show two (negative) peaks in the same direction. In general, most of the observational features are captured in our simulated spirals.

It should be noted that the DMSP trajectory is at ~800 km in altitude, below the auroral acceleration region in our simulation. The density and temperature observed by DMSP satellite are ionospheric values ($n_e \approx 10^4 \, \text{cm}^{-3}$, $T_e \approx 3 \times 10^3 \, \text{K}$), and are different from those in our simulation. The correlation between our simulation and observation can be interpreted as the increase of the ionization and heating of the ionospheric component resulted from the enhancement of electron precipitation. The ion horizontal velocity observed by DMSP satellite can be assumed to be the advection speed of the magnetic field lines. To explain this data, we use the x component of $\mathbf{E} \times \mathbf{B}$ drift velocity in panel (h).

4. Discussion and Conclusions

In this paper, we perform 3-D PIC simulations to study the formation of auroral spiral structures. Our simulation shows that precipitating electrons accelerated during reconnection (within the auroral acceleration region) develop a narrow arc-like pattern. Later, the arc morphology is modified by flux ropes generated through secondary oblique tearing instability. The simulated process resembles the observed evolution of a real auroral arc, providing an explanation to the auroral spiral structure formation. These secondary tearing modes are pronounced only in the lower altitude; this altitude dependence is consistent with the 3-D nature of reconnection x-line in Y. H. Liu et al. (2019) and Huang, Liu, et al. (2020). Moreover, this study predicts that when the auroral acceleration region is too short, the auroral arc will be stable, and no spiral structure can form. The rotational sense of the spirals is determined by the electron kinetic physics associated with reconnection and tearing modes. When the
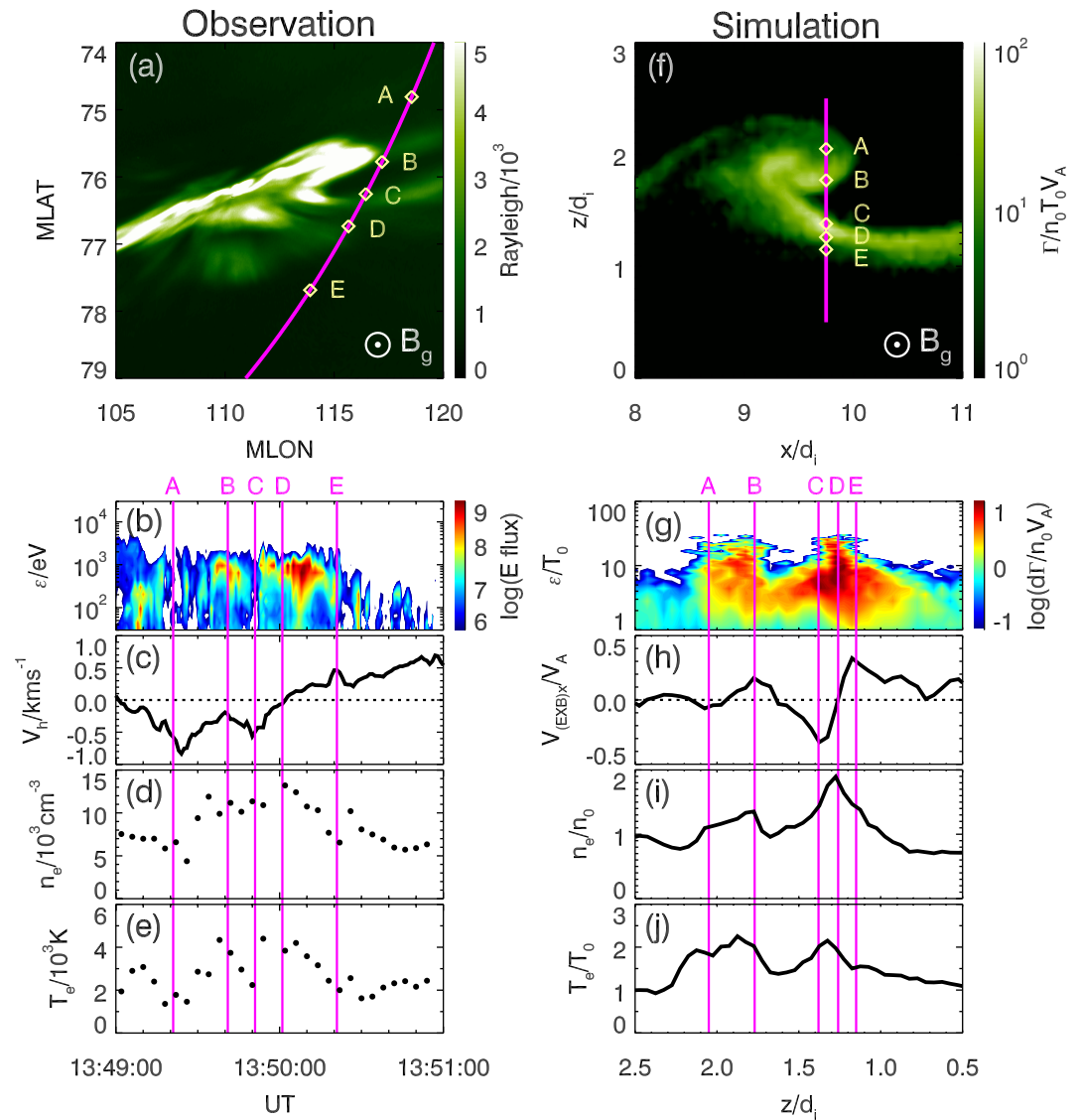
Figure 4. A comparison between the observation (left) and simulation (right). Panel (a) shows the optical emission intensity of the auroral spiral observed at 13:49:40 on 24 December 2003 by Yellow River Station. The magenta curve represents the trajectory of DMSP satellite. Both the emission intensity and the DMSP trajectory are mapped to 150 km altitude. Panels (b–e) plot the color contour of electron differential energy flux (E flux, $eV \cdot cm^{-2} \cdot s^{-1} \cdot str^{-1} \cdot eV^{-1}$) at different energy ε, ion horizontal velocity V_h (perpendicular to the satellite trajectory, with eastward direction being positive), electron density n_e, and electron temperature T_e observed by DMSP satellite. Panel (f) shows one simulated spiral. Panels (g–j) plot the color contour of electron differential energy flux (d Γ) at different energy ε/T_0, x component of $\mathbf{E} \times \mathbf{B}$ drift velocity $V_{(\mathbf{E}\times\mathbf{B})x}/V_A$, electron density n_e/n_0, and electron temperature T_e/T_0 along the magenta line in panel (f). Quantities at the denominators in panels (f–j) show the normalization.

direction of the guide field is reversed, the rotational sense of the spirals also reverses, explaining the observed difference at the northern versus southern hemisphere.

Previous 2-D simulations indicated that tearing instability and reconnection do persist with an extremely large guide field (Y. H. Liu et al., 2014; TenBarge et al., 2014), which is closer to the condition of auroral acceleration region. The thickness of the intensified current layer during reconnection with a more realistic mass ratio and larger guide field remains on the d_e-scale (Goldman et al., 2011; Y. H. Liu et al., 2014). The formation of spirals takes about $10\Omega_i^{-1}$ in our simulation, which corresponds to ~1 s if we assume the magnetic field associated with the FAC sheet is $B_0 = 100$ nT. It is too short compared to that in observations (Davis & Hallinan, 1976), but could be overcome by the slower growth rate of tearing instability by a factor of 100 because of $B_g/B_0 \approx 100$. Then the

formation time of spirals would be ∼100 s, comparable to observations. Therefore, the main results of current work can be extrapolated to the system with more realistic parameters.

The most cited explanation of auroral spirals is the current sheet instability proposed by Hallinan (1976) and further advanced by Partamies, Freeman, and Kauristie (2001). Lysak and Song (1996) studied the coupling between the flow shear and the resulting magnetic shear and argued that spirals can form through the current sheet instability in the case with large height-integrated conductivity on the ionospheric side. In contrast, the key physics underlying our simulated spirals is the secondary tearing instability. The ionospheric feedback is not that critical in our explanation, and this statement is confirmed by a similar result of a companion simulation (Figure S4 in Supporting Information S1) that has an open boundary for both particles and fields on the ionospheric side.

Otto and Birk (1992) suggested the potential role of tearing modes using resistive-MHD simulations. However, the electron kinetic physics, that is critical in explaining the rotational sense of spirals in our model, is absent in their explanation. The collisionless tearing instability is also argued to be the plausible source of vortex auroral structures using a reduced MHD model including the dispersive effect from electron inertia (Chaston, 2015; Seyler, 1990; Seyler Jr, 1988). However, the vortex structures in these studies are associated with flow vortices that have a rotational sense consistent with curls, instead of spirals. The rotational sense of the flow shear near the separatrices in our simulation and DMSP observation (Figure 4) are also consistent with that in Seyler's and Chaston's. To resolve this seemly inconsistent rotation between the flow shear and spiral, it is important to note that the rotational sense of spirals describes the swirling pattern of a 2-D projection, which does not need to be consistent with the local plasma flow shear. Finally, although not appearing in the simulation presented here, curl-like structures associated with smaller Debye-length-scale vortices can also develop during reconnection with a stronger guide field in PIC simulations (Figure 5b in Y. H. Liu et al. (2014)).

Our mechanism can explain periodic-looking multiple spiral structures which evolve from a narrow arc. Although large-scale spirals may be generated between two primary reconnection x-lines or through the growth of flux ropes ($x \approx -3d_i$ in Movie S1), it is still a challenge to exclusively explain the solitary, large-scale (hundreds of kilometers and larger) spiral. We leave this issue as an open question. Even though 3-D PIC simulations, given the challenges with realistic parameters, do not encompass the entirety of the problem, the presented simulations do show the value of the tearing instability in understanding auroral spiral structures. Direct evidence of reconnection in the auroral acceleration region could be possible using satellites of higher spatial and temporal resolutions in the future.

Data Availability Statement

The simulation data and scripts used to plot the figures are available at National Space Science Data Center, National Science and Technology Infrastructure of China (https://dx.doi.org/10.12176/01.99.00714). The data of Special Sensor for Particle Flux (SSJ/4) and Special Sensor Ions Electrons and Scintillation (SSIES) aboard DMSP satellite are from National Centers for Environmental Information of NOAA (https://www.ngdc.noaa.gov/stp/satellite/dmsp/).

References

Borovsky, J. E., Birn, J., Echim, M. M., Fujita, S., Lysak, R. L., Knudsen, D. J., et al. (2020). Quiescent discrete auroral arcs: A review of magnetospheric generator mechanisms. *Space Science Reviews*, *216*(1), 1. https://doi.org/10.1007/s11214-019-0619-5

Bowers, K. J., Albright, B. J., Bergen, B., Yin, L., Barker, K. J., & Kerbyson, D. J. (2008). 0.374 pflop/s trillion-particle kinetic modeling of laser plasma interaction on roadrunner. In *Sc'08: Proceedings of the 2008 acm/ieee conference on supercomputing* (pp. 1–11).

Chaston, C. (2015). Magnetic reconnection in the auroral acceleration region. *Geophysical Research Letters*, *42*(6), 1646–1653. https://doi.org/10.1002/2015gl063164

Daughton, W., Roytershteyn, V., Karimabadi, H., Yin, L., Albright, B., Bergen, B., & Bowers, K. (2011). Role of electron physics in the development of turbulent magnetic reconnection in collisionless plasmas. *Nature Physics*, *7*(7), 539–542. https://doi.org/10.1038/nphys1965

Daughton, W., Scudder, J., & Karimabadi, H. (2006). Fully kinetic simulations of undriven magnetic reconnection with open boundary conditions. *Physics of Plasmas*, *13*(7), 072101. https://doi.org/10.1063/1.2218817

Davis, T., & Hallinan, T. (1976). Auroral spirals, 1. Observations. *Journal of Geophysical Research*, *81*(22), 3953–3958. https://doi.org/10.1029/ja081i022p03953

Drake, J., & Lee, Y. (1977). Kinetic theory of tearing instabilities. *The Physics of Fluids*, *20*(8), 1341–1353. https://doi.org/10.1063/1.862017

Eastwood, J., Mistry, R., Phan, T., Schwartz, S., Ergun, R., Drake, J., et al. (2018). Guide field reconnection: Exhaust structure and heating. *Geophysical Research Letters*, *45*(10), 4569–4577. https://doi.org/10.1029/2018gl077670

Elphinstone, R., Murphree, J., Hearn, D., Cogger, L., Sandahl, I., Newell, P., et al. (1995). The double oval uv auroral distribution: 1. Implications for the mapping of auroral arcs. *Journal of Geophysical Research*, *100*(A7), 12075–12092. https://doi.org/10.1029/95ja00326

Ergun, R., Carlson, C., McFadden, J., Delory, G., Strangeway, R., & Pritchett, P. (2000). Electron-cyclotron maser driven by charged-particle acceleration from magnetic field-aligned electric fields. *The Astrophysical Journal*, *538*(1), 456–466. https://doi.org/10.1086/309094

Ergun, R., Carlson, C., McFadden, J., Mozer, F., & Strangeway, R. (2000). Parallel electric fields in discrete arcs. *Geophysical Research Letters*, *27*(24), 4053–4056. https://doi.org/10.1029/2000gl003819

Goldman, M., Lapenta, G., Newman, D., Markidis, S., & Che, H. (2011). Jet deflection by very weak guide fields during magnetic reconnection. *Physical Review Letters*, *107*(13), 135001. https://doi.org/10.1103/physrevlett.107.135001

Hallinan, T. (1976). Auroral spirals, 2. Theory. *Journal of Geophysical Research*, *81*(22), 3959–3965. https://doi.org/10.1029/ja081i022p03959

Hardy, D. A. (1984). Precipitating electron and ion detectors (ssj/4) for the block 5d/flights 6-10 dmsp satellites: Calibration and data presentation. Rep. AFGL-TR-84-0317.

Hu, Z.-J., Yang, H., Huang, D., Araki, T., Sato, N., Taguchi, M., et al. (2009). Synoptic distribution of dayside aurora: Multiple-wavelength all-sky observation at yellow river station in Ny-Ålesund, Svalbard. *Journal of Atmospheric and Solar-Terrestrial Physics*, *71*(8–9), 794–804. https://doi.org/10.1016/j.jastp.2009.02.010

Hu, Z.-J., Yang, H.-G., Hu, H.-Q., Zhang, B.-C., Huang, D.-H., Chen, Z.-T., & Wang, Q. (2013). The hemispheric conjugate observation of post-noon "bright spots"/auroral spirals. *Journal of Geophysical Research: Space Physics*, *118*(4), 1428–1434. https://doi.org/10.1002/jgra.50243

Huang, K., Liu, Y.-H., Lu, Q., & Hesse, M. (2020). Scaling of magnetic reconnection with a limited x-line extent. *Geophysical Research Letters*, *47*(19), e2020GL088147. https://doi.org/10.1029/2020gl088147

Huang, K., Lu, Q.-M., Wang, R.-S., & Wang, S. (2020). Spontaneous growth of the reconnection electric field during magnetic reconnection with a guide field: A theoretical model and particle-in-cell simulations. *Chinese Physics B*, *29*(7), 075202. https://doi.org/10.1088/1674-1056/ab8da0

Johnson, J. R., Wing, S., & Delamere, P. A. (2014). Kelvin Helmholtz instability in planetary magnetospheres. *Space Science Reviews*, *184*(1–4), 1–31. https://doi.org/10.1007/s11214-014-0085-z

Karlsson, T., Andersson, L., Gillies, D., Lynch, K., Marghitu, O., Partamies, N., et al. (2020). Quiet, discrete auroral arcs—Observations. *Space Science Reviews*, *216*(1), 16. https://doi.org/10.1007/s11214-020-0641-7

Keiling, A., Angelopoulos, V., Runov, A., Weygand, J., Apatenkov, S., Mende, S., et al. (2009). Substorm current wedge driven by plasma flow vortices: Themis observations. *Journal of Geophysical Research*, *114*(A1). https://doi.org/10.1029/2009ja014114

Keiling, A., Angelopoulos, V., Weygand, J., Amm, O., Spanswick, E., Donovan, E., et al. (2009). Themis ground-space observations during the development of auroral spirals. *Annales Geophysicae*, *27*(11), 4317–4332. https://doi.org/10.5194/angeo-27-4317-2009

Kleva, R. G., Drake, J., & Waelbroeck, F. (1995). Fast reconnection in high temperature plasmas. *Physics of Plasmas*, *2*(1), 23–34. https://doi.org/10.1063/1.871095

Lanchester, B. (2017). Some remaining mysteries in the aurora. *Astronomy and Geophysics*, *58*(3), 3–17. https://doi.org/10.1093/astrogeo/atx098

Le, A., Egedal, J., Ohia, O., Daughton, W., Karimabadi, H., & Lukin, V. (2013). Regimes of the electron diffusion region in magnetic reconnection. *Physical Review Letters*, *110*(13), 135004. https://doi.org/10.1103/physrevlett.110.135004

Liu, Y.-H., Daughton, W., Karimabadi, H., Li, H., & Peter Gary, S. (2014). Do dispersive waves play a role in collisionless magnetic reconnection? *Physics of Plasmas*, *21*(2), 022113. https://doi.org/10.1063/1.4865579

Liu, Y. H., Daughton, W., Karimabadi, H., Li, H., & Roytershteyn, V. (2013). Bifurcated structure of the electron diffusion region in three-dimensional magnetic reconnection. *Physical Review Letters*, *110*(26), 265004. https://doi.org/10.1103/physrevlett.110.265004

Liu, Y.-H., Li, T., Hesse, M., Sun, W., Liu, J., Burch, J., et al. (2019). Three-dimensional magnetic reconnection with a spatially confined x-line extent: Implications for dipolarizing flux bundles and the dawn-dusk asymmetry. *Journal of Geophysical Research: Space Physics*, *124*(4), 2819–2830. https://doi.org/10.1029/2019ja026539

Lu, Q., Wang, R., Xie, J., Huang, C., Lu, S., & Wang, S. (2011). Electron dynamics in collisionless magnetic reconnection. *Chinese Science Bulletin*, *56*(12), 1174–1181. https://doi.org/10.1007/s11434-011-4440-0

Lui, A., Venkatesan, D., & Murphree, J. (1989). Auroral bright spots on the dayside oval. *Journal of Geophysical Research*, *94*(A5), 5515–5522. https://doi.org/10.1029/ja094ia05p05515

Lysak, R. L., & Song, Y. (1996). Coupling of Kelvin-Helmholtz and current sheet instabilities to the ionosphere: A dynamic theory of auroral spirals. *Journal of Geophysical Research*, *101*(A7), 15411–15422. https://doi.org/10.1029/96ja00521

Marklund, G., Karlsson, T., Blomberg, L., Lindqvist, P.-A., Fälthammar, C.-G., Johnson, M., et al. (1998). Observations of the electric field fine structure associated with the westward traveling surge and large-scale auroral spirals. *Journal of Geophysical Research*, *103*(A3), 4125–4144. https://doi.org/10.1029/97ja00558

Murphree, J., & Elphinstone, R. (1988). Correlative studies using the Viking imagery. *Advances in Space Research*, *8*(9–10), 9–19. https://doi.org/10.1016/0273-1177(88)90108-1

Otto, A., & Birk, G. (1992). The dynamical evolution of small-scale auroral arc phenomena due to a resistive instability. *Journal of Geophysical Research*, *97*(A6), 8391–8397. https://doi.org/10.1029/92ja00013

Partamies, N., Freeman, M., & Kauristie, K. (2001). On the winding of auroral spirals: Interhemispheric observations and Hallinan's theory revisited. *Journal of Geophysical Research*, *106*(A12), 28913–28924. https://doi.org/10.1029/2001ja900093

Partamies, N., Kauristie, K., Pulkkinen, T., & Brittnacher, M. (2001). Statistical study of auroral spirals. *Journal of Geophysical Research*, *106*(A8), 15415–15428. https://doi.org/10.1029/2000ja900172

Paschmann, G., Haaland, S., Treumann, R., Amm, O., Birn, J., & Borovsky, J. (2002). Auroral plasma physics. *Space Science Reviews*, *103*(1–4).

Pritchett, P., & Coroniti, F. V. (2004). Three-dimensional collisionless magnetic reconnection in the presence of a guide field. *Journal of Geophysical Research*, *109*(A1), A01220. https://doi.org/10.1029/2003ja009999

Rich, F. J. (1994). Users guide for the topside ionospheric plasma monitor (SSIES, SSIES-2 and SSIES-3) on spacecraft of the defense meteorological satellite program (Vol. *1*). Technical description.

Sauppe, J. P., & Daughton, W. (2018). Kinetic-scale flux rope reconnection in periodic and line-tied geometries. *Physics of Plasmas*, *25*(1), 012901. https://doi.org/10.1063/1.5007860

Seyler, C. E. (1990). A mathematical model of the structure and evolution of small-scale discrete auroral arcs. *Journal of Geophysical Research*, *95*(A10), 17199–17215. https://doi.org/10.1029/ja095ia10p17199

Seyler, C. E., Jr. (1988). Nonlinear 3-D evolution of bounded kinetic Alfvén waves due to shear flow and collisionless tearing instability. *Geophysical Research Letters*, *15*(8), 756–759. https://doi.org/10.1029/gl015i008p00756

TenBarge, J., Daughton, W., Karimabadi, H., Howes, G., & Dorland, W. (2014). Collisionless reconnection in the large guide field regime: Gyrokinetic versus particle-in-cell simulations. *Physics of Plasmas*, *21*(2), 020708. https://doi.org/10.1063/1.4867068

Weimer, D., & Gurnett, D. (1993). Large-amplitude auroral electric fields measured with DE 1. *Journal of Geophysical Research*, *98*(A8), 13557–13564. https://doi.org/10.1029/93ja00793